La Paz Icefield 02205, 02224, 02226, 02436, 03632, 04841

Unbrecciated basalt

1226.3, 252.5, 244.1, 59.0, 92.6, 56 g

Figure 1: LAP 02205 as found in the LaPaz Icefield. Scale bar at base of counter is in cm.

Introduction

La Paz Icefield (LAP) 02205 (Fig. 1) and its paired masses, LAP 02224, 226, 436, LAP 03632, and LAP 04841 (Fig. 2), are an unbrecciated mare basalt that total ~1930 g. These meteorites were discovered in the LaPaz Icefield in the 2002, 2003, and 2004 ANSMET field seasons and their recovery locations define a linear trend (Fig. 3), which together with their textural, mineralogical, and petrologic similarities argue for pairing. These meteorites represent a unique basaltic composition not represented in the Apollo collections, and the first unbrecciated mare basaltic meteorite from Antarctica.

Petrography

The LAP meteorites all show similar texture and mineralogy. They are all medium to coarse-grained subophitic basalts, with a dominance of pyroxene, plagioclase and ilmenite (Table 1 and Fig. 4 and 5). Each contains traces of olivine, spinel, troilite, silica, baddeleyite, and

metal. These LAP meteorites also contain heterogeneous melt veins and pockets whose composition is similar to the bulk composition of the rock with only limited variation.

Figure 2: LAP 02224, 02226, 02436 and 03632 as found in the ice (clockwise from upper left).

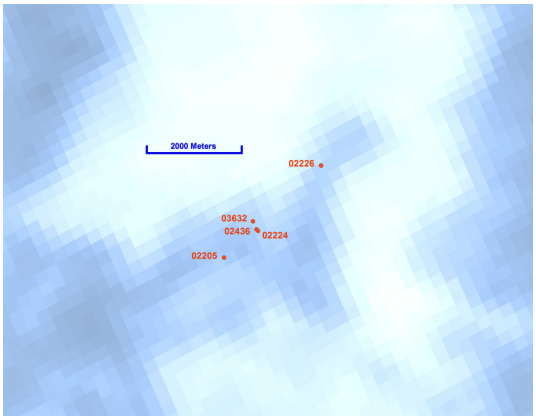

Figure 3: Relative positions of the LAP lunar basaltic meteorites, as discovered in the LaPaz Icefield.

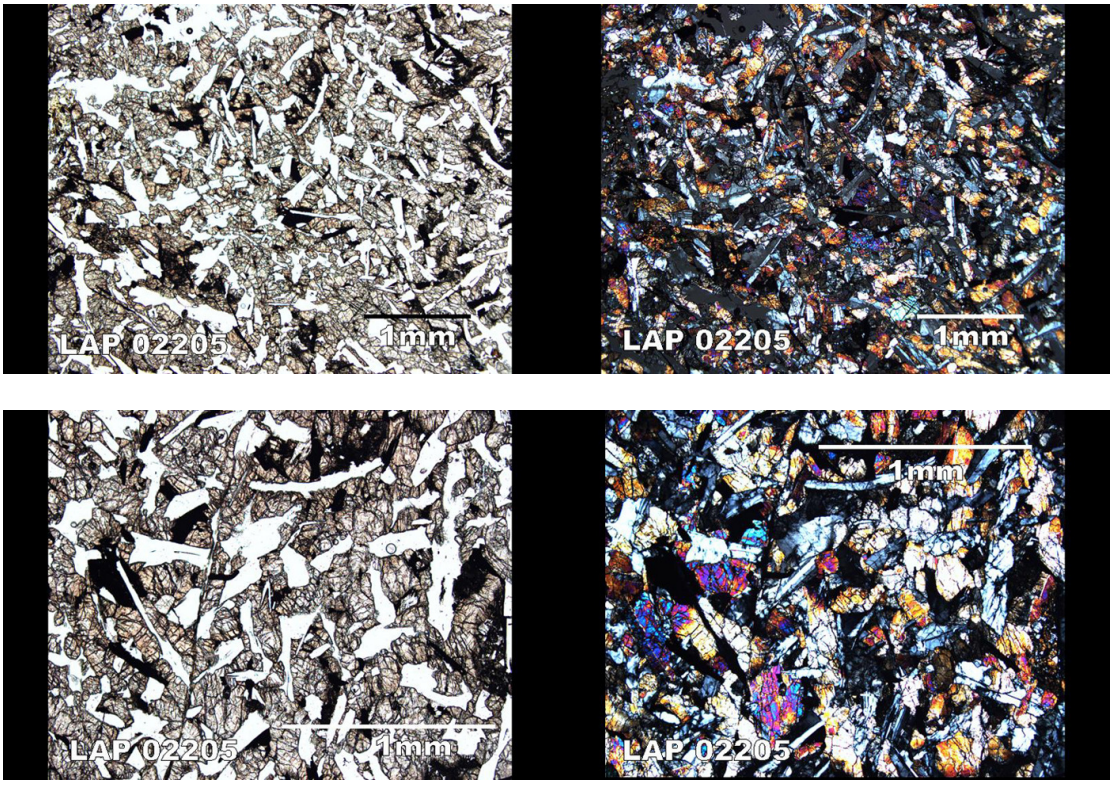

Figure 4: Plane polarized light (left side) and cross nicols (right side) photomicrographs of LAP 02205 illustrating the prevalence of pyroxene (grey) and plagioclase feldspar (white), as well as ilmenite and spinel.

Mineralogy

Several studies have focused on the mineralogy of these basaltic meteorites (Anand et al., 2005; Righter et al., 2005; Zeigler et al., 2005; Day et al., 2006; Joy et al., 2005; Hill et al., 2009). The mineralogy of the last of the six masses to be recovered – LAP 04841 – has been well documented but not covered as extensively in this summary due to the similarity to the other 5 masses (Hill et al., 2009).

Olivine: Olivines are generally subhedral in shape although some grains have a skeletal habit with subhedral outlines. The olivine compositions range from Fo_{53} to Fo_{62} in the cores to Fo_{46} to Fo_{57} in the rims (Fig. 6). The modal proportion of olivine in four LAP meteorites ranges from 1.1 to 3.6% (Table 1). Righter et al. (2005) proposed that the olivines are out of equilibrium with the bulk rock composition and therefore are xenocrysts.

Pyroxene: The pyroxene is either intersertile or enclosing plagioclase within all of the rocks. Pyroxene grains have strong chemical variation from pigeonite to ferroaugite (Fig. 7). The ferroaugite has strong Fe enrichment and Mg depletion towards the rims of grains and they contain pigeonite cores. Thin augite lamellae are also present within some grains indicative of slow cooling rates. This feature results from subsolidus exsolution of pigeonite into orthopyroxene and augite. LAP basalt pyroxenes also exhibit clear affinity with lunar Fe/Mn ratios (Fig. 8).

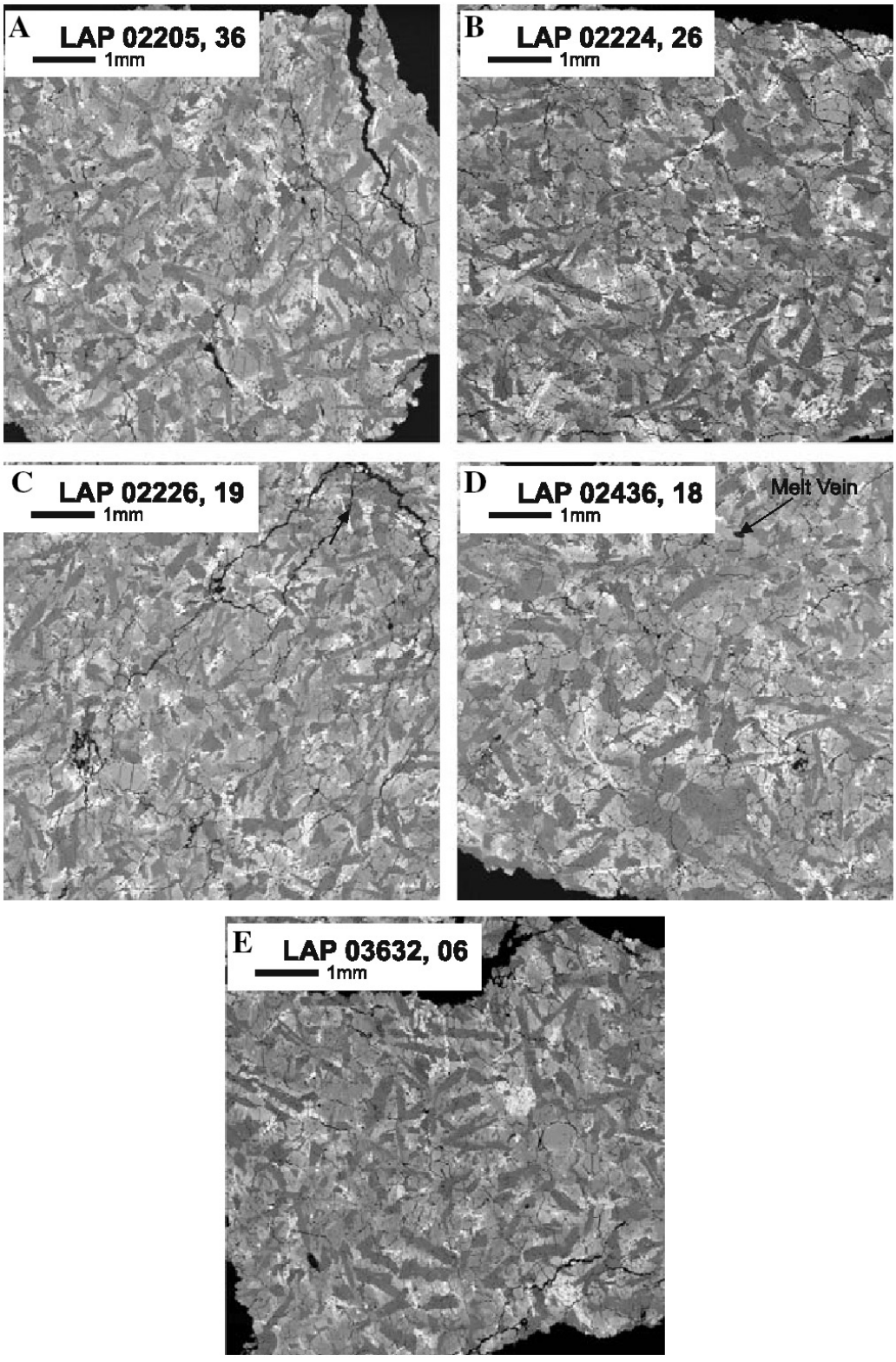

Figure 5: Back scattered electron images of five of the La Paz lunar basaltic meteorites, illustrating the textures within these paired samples (from Day et al., 2006). Textures documented in LAP 04841 are identical to these 5 masses (Hill et al., 2009).

Table 1: Modal analysis of the LAP meteorites

	LAP 02205	***LAP 02226***	***LAP 02224***	***LAP 02436***	***LAP 03632***	***LAP 02205***	***LAP 02205***	***LAP 02226***	***LAP 02224***	***LAP 02436***	***LAP 04841***
reference	1	1	1	1	1	2	3	3	3	3	4
Pyroxene	43.9	51.2	52.9	53.1	50.7	56.9	51.5	50.5	46.9	46.6	56.20
Plagioclase	45.3	36.3	39.2	34.7	39.1	33.1	31.9	32.1	32.3	34.6	31.90
Ilmenite	3.7	5.1	3.8	4.6	3.1	3.3	3.48	3.91	3.86	3.99	3.34
Olivine	1.1	1.7	1.6	1.5	2.7	1.2	2.33	2.71	3.63	3.20	1.54
Spinel	1.5	1.0	0.7	0.8	0.2	0.4	0.34	0.45	0.40	0.39	1.00
Phosphate	0.7	1.4	0.8	1.7	0.7	0.3	2.14	2.09	1.78	2.00	n.r.
Troilite	1.4	0.6	0.3	1.3	1.1	0.2	0.25	0.24	0.24	0.22	0.07
Fay. symp.	2.5	2.8	0.7	2.3	2.4	1.5	3.09	2.90	3.58	4.83	5.27
Other#	tr	tr	tr	tr	tr	tr	0.10	0.20	2.20	-	0.72

#Fe metal, melt veins, and baddeleyite are present in trace amounts in all samples.
References: 1) Righter et al. (2005), 2) Anand et al. (2005), 3) Ziegler et al. (2005); 4) Hill et al. (2009).

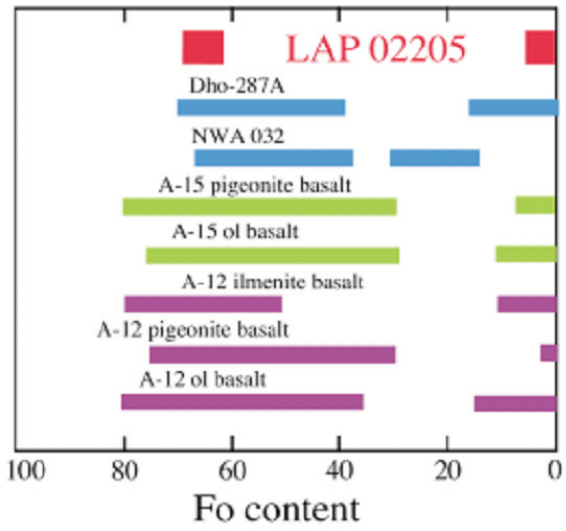

Figure 6: Olivine composition in LAP 02205 compared to Dho-287A, NWA032, and other Apollo mare basalt samples.

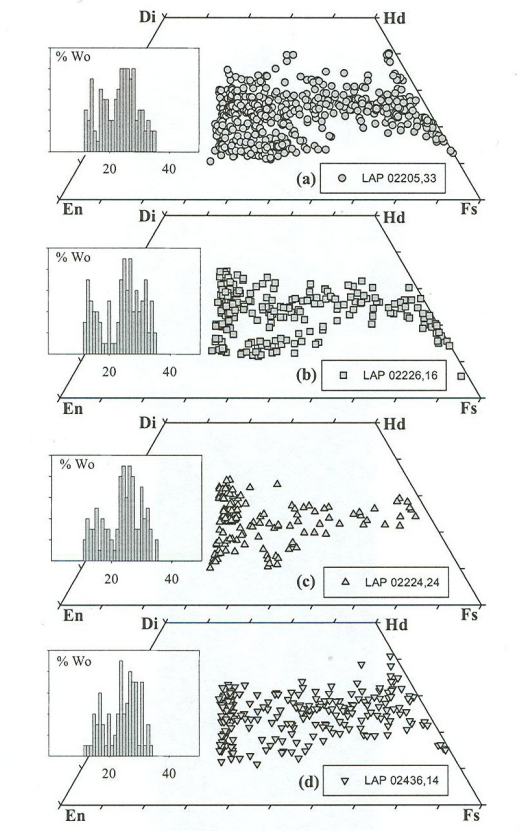

Figure 7: Pyroxene quadrilateral diagrams showing the range of pyroxene from pigeonite and augite cores to more Fe-rich rims (from Zeigler et al., 2005).

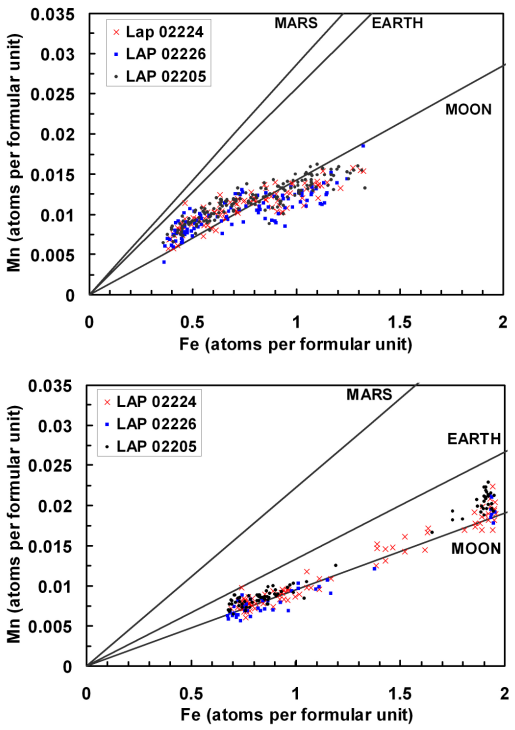

Figure 8: Fe/Mn ratios for pyroxenes for LAP 02205, 02224 and 02226 (from Joy et al., 2005).

Plagioclase: Plagioclase is a dominant component in the LAP meteorites and ranges from 32 to 45 modal percent (Table 1). It occurs commonly as laths but in some cases has a blocky texture. The plagioclase compositions of the LAP meteorites range from An_{85} to An_{89}.

Ilmenite: Ilmenite occurs within the LAP meteorites as the most dominant opaque. The ilmenites co-precipitated with pyroxene and plagioclase from the cooling magma as lath-like crystals. Modal percent of ilmenite within these meteorites ranges from 3.1% to 5.1% (Table 1). Ilmenite in these samples contain very low concentrations of MgO with a range from 0.02 to 0.24 wt. %.

Baddeleyite: Occurs in association with ulvospinels, ilmenite and troilite, and is typically 20 to 40 µm in size.

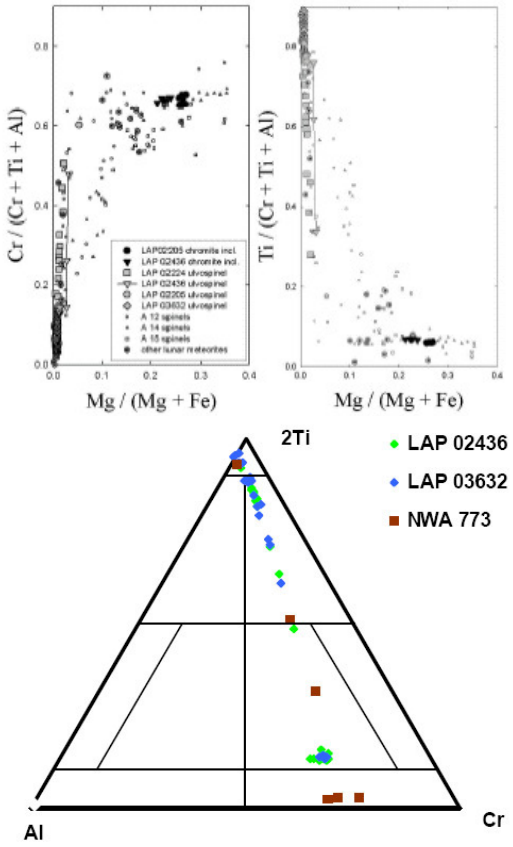

Figure 9a: Range of spinel compositions in LAP meteorites with Cr-rich spinel found as inclusions in olivine, followed by later Cr ulvospinel that co-crystallizes with ilmenite (from Righter et al., 2005).Figure 9b: Transition of Cr-rich to Ti-rich spinels in NWA 773 and LAP basalt series of samples (from Hallis et al., 2007).

Spinel: Spinel in these samples make up 0.2 to 1.5 modal % (Table 1). Ulvospinel occurs as equant grains with little zonation. Small chromite inclusions are present within olivine phenocrysts and are thought to have been the earliest spinels to crystallize. Chromite crystallization was followed by Cr – poor ulvospinel (Fig. 9).

Metal: Metal grains are small (10-20 µm) and are commonly associated with spinel and sulphide within the LAP meteorites. There is a large amount of compositional variation within the metal grains throughout these rocks (Day et al.,

2005, 2006), but it is thought to be indigenous to the sample, rather than affected by meteoritic contamination (Fig. 10).

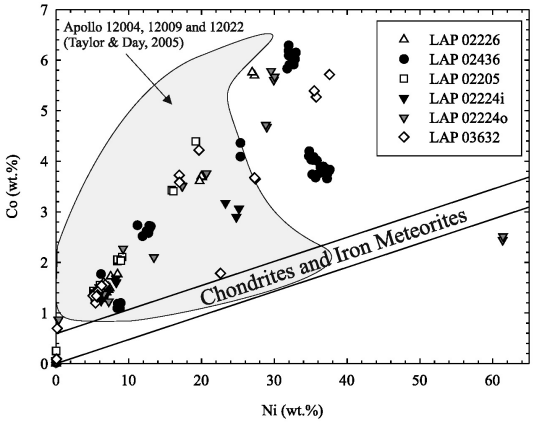

Figure 10: Ni vs. Co (all in wt%) for metal grains in the LaPaz basalt suite. The extensive variation is indigenous tot he sample rather than contributed by meteoritic contamination (Day et al., 2006).

Troilite: Troilite is present in trace amounts and with equant morphology. Troilite is typically found in association with oxide grains and in some cases with metal.

Silica: The LAP meteorites contain cristobalite found as trace amounts, and usually associated with late stage mesostasis or symplectitic fayalite, plagioclase and metal (Fig. 11).

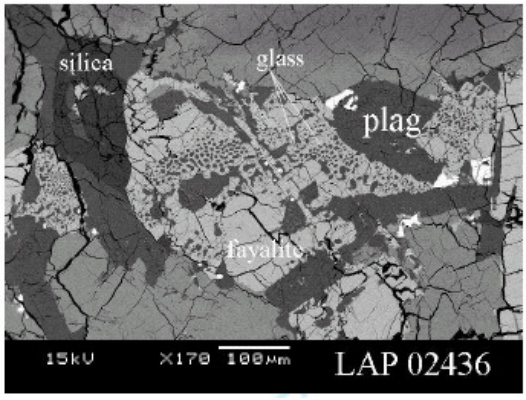

Figure 11: Symplectitic texture in the mesostasis of LAP 02436, involving fayalite and glass (from Righter et al., 2005).

Melt veins: Ubiquitous melt veins are heterogeneous in composition and commonly contain areas with relict mineral grains.

Textural studies of the La Paz lunar basaltic meteorites indicate cooling rates (based on plagioclase, pyroxene and ilmenite) of 0.1 to 0.3 C/hr), consistent with an origin near the middle of a slowly cooled lava flow (Day and Taylor, 2007). These cooling rates are in general agreement, but slightly lower than those inferred by Koizumi et al. (2005) based on experimental studies.

Chemistry

Several groups have reported INAA and ICP-MS analyses of relatively small (35 to 50 mg) chips of LAP 02205 and its paired samples (Table 2).

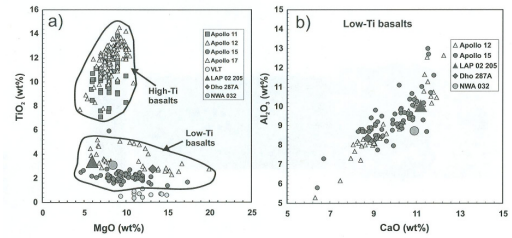

Figure 12: LAP basalts fall within the low Ti basalt field with respect to TiO_2, MgO, CaO and Al_2O_3 (from Zeigler et al., 2005).

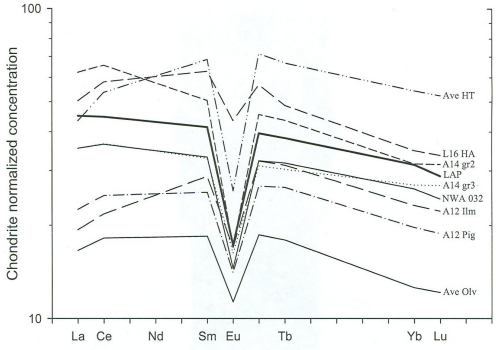

Figure 13: Rare earth element diagram for LAP 02205 compared to many other Apollo basalts and NWA032 (from Zeigler et al., 2005).

TiO_2 compositions are similar to low Ti basalts such as Apollo 12 ilmenite and olivine basalts (Fig. 12). They also show relatively high Al_2O_3 and seem to be depleted in MgO compared to the other lunar samples. Europium anomalies are similar to other mare basalts, except that the absolute REE contents are high, suggesting a more evolved or fractionated basalt compared to many Apollo mare basalts (Fig. 13).

Table 2a. Chemical composition of LAP 02205

reference	1	2	2	2	2	2	2	2	3	4	5
										melt vein	
weight	-	35.3	40.2	40.2	34.5	41.3	48.9	avg	50	avg	
split		,20-1	,20-2	,20-3	,24-1	,24-2	,24-3				,21
technique	b	d,e	d,e	d,e	d,e	d,e	d,e	d,e	b		d,e
SiO_2 %	44.5	45	45.3	45.2	45.3	44.6	45.2	45.1	45.2	44.08	46.0
TiO_2	3.43	3.34	3.33	3.34	2.99	3.28	3.13	3.23	3.38	4.18	3.11
Al_2O_3	10.13	9.84	10.18	10.48	9.63	8.98	10.2	9.9	10	14.52	9.95
Cr_2O_3		0.26	0.22	0.26	0.33	0.32	0.33	0.29	0.19	0.16	0.29
FeO	21.69	22.9	22.8	21.9	21.7	23.3	21.6	22.3	23.2	18	21.8
MnO	0.28	0.28	0.3	0.29	0.28	0.34	0.32	0.3	0.23	0.22	0.32
MgO	5.58	5.87	5.46	5.69	7.17	7.11	6.68	6.34	5.99	5.41	6.32
CaO	11.23	11.1	11.2	11.4	11.1	10.5	11.3	11.1	11.2	11.56	11.4
Na_2O	0.42	0.39	0.42	0.41	0.38	0.36	0.39	0.39	0.33	0.56	0.39
K_2O		0.08	0.09	0.07	0.06	0.07	0.06	0.07	0.11	0.13	0.10
P_2O_5	0.12	0.11	0.11	0.1	0.09	0.08	0.08	0.09	0.12	0.17	0.17
S %											0.16
sum	97.38	99.17	99.41	99.14	99.03	98.94	99.29	99.11	99.95	98.99	100.00
Sc ppm		59	58	57.8	59.5	58.9	60.4	59	58.6		52.8
V									129		92
Cr		1751	1511	1767	2290	2180	2230	1962			1625
Co		34.6	33.9	34	37.8	40.4	37	36.3	37.3		35.4
Ni		0	50	30	50	30	30	32	27.6		42.4
Cu											18.6
Zn											27.5
Ga											3.74
Ge											
As											
Se											
Rb									2.1		1.67
Sr		150	160	190	130	130	110	144	135.3		109
Y									73.2		57.0
Zr		200	260	250	210	150	140	199	200.3		172
Nb									14.7		11.9
Mo											
Ru									3.6		
Rh									1.2		
Pd ppb									8.3		

Ag ppb									
Cd ppb									
In ppb									
Sn ppb									
Sb ppb									
Te ppb									
Cs ppm								0.1	0.03
Ba	166	154	150	124	134	152	147	164.7	122
La	14.7	15.3	14.2	11.6	15.3	14.6	14.4	13.4	9.97
Ce	38.3	39.6	36.6	32.2	37	36	36.7	37.31	26.3
Pr								5.15	4.04
Nd	25	28	23	20	27	20	24	25.12	19.1
Sm	8.6	8.89	8.35	7.04	8.51	8.19	8.28	7.56	6.05
Eu	1.36	1.41	1.36	1.2	1.26	1.29	1.31	1.24	0.98
Gd								9.95	7.81
Tb	1.89	2.02	1.91	1.63	1.95	1.86	1.88	1.93	1.44
Dy								12.08	9.35
Ho								2.45	2.00
Er								6.71	5.40
Tm								0.94	0.84
Yb	7.3	7.4	7	6.1	7	6.7	6.9	6.37	5.30
Lu	0.99	1.03	0.96	0.83	0.95	0.94	0.95	0.88	0.82
Hf	6.27	6.42	6.06	5.1	5.71	5.5	5.84	5.39	4.50
Ta	0.8	0.8	0.79	0.69	0.67	0.69	0.74	0.77	0.60
W ppb								0.2	
Re ppb									
Os ppb									
Ir ppb								1.8	
Pt ppb								31.5	
Au ppb									
Th ppm	2.24	2.34	2.2	1.79	2.01	1.93	2.08	2.33	1.79
U ppm	0.61	0.52	0.67	0.55	0.53	0.42	0.54	0.55	0.45

technique (a) ICP-AES, (b) ICP-MS, (c) IDMS, (d) fused bead EMPA, (e) INAA, (f) RNAA, (g) SSM

References: 1) Joy et al. (2005); 2) Zeigler et al. (2005); 3) Anand et al. (2005); 4) Righter et al. (2005); 5) Day et al. (2006).

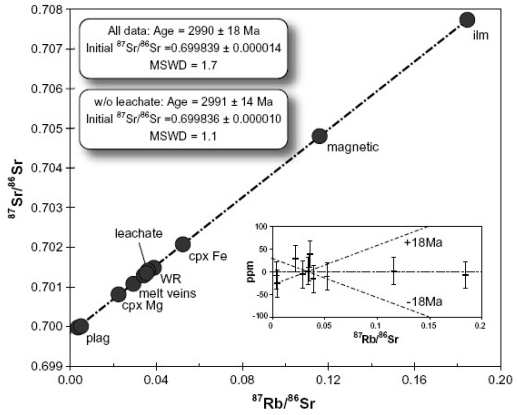

Figure 14: Rb-Sr whole rock and mineral separate isochron for LAP 02205 (from Rankenburg et al., 2007).

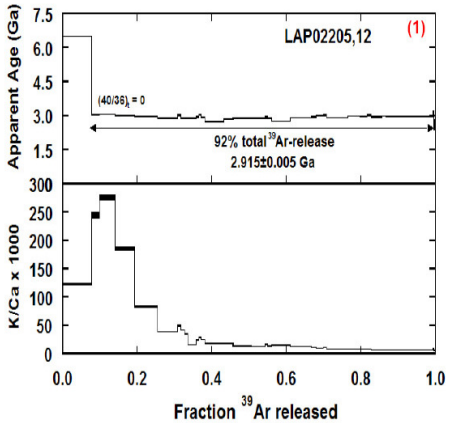

Figure 15: Ar plateau age and K/Ca ratio for LAP 02205 (Fernandes and Burgess, 2006 and Fernandes et al., 2009).

Table 2b. Light and/or volatile elements for LAP 02205

	Anand05
Li ppm	11.7
Be	1.37
C	
S	
F ppm	
Cl	
Br	
I	
Pb ppm	1
Hg ppb	
Tl	
Bi	

Platinum group element analyses of the LAP basalts (Day et al., 2006) have been used to argue for the addition of late chondritic material to the mantle of the Moon after a giant impact and lunar core formation. Although this simple approach is based on comparisons between lunar and terrestrial basalt PGE systematics, it does not apparently assess or take into account differences in sulfide saturation between lunar and terrestrial basalts. Nonetheless these high quality and low concentration PGE data for the lunar basalts provides useful constraints of the origin of the Moon.

Radiogenic age dating

Several groups have reported radiometric age determinations of the LAP basalts. A whole rock Rb-Sr isochron based on mineral separates from LAP 02205 yields an age of 2.990 (±0.018) Ga (Fig. 14; Rankenburg et al., 2007) which is identical within error to the age obtained by Shih et al. (2005) of 3.02 (±0.03) Ga. Ar dating of LAP 02205 whole rock material yields an age of 2.936 Ga. The latter age is nearly identical to that obtained using UV laser Ar dating of LAP 02205 samples yields an age of 2.915 Ga (Fig. 15; Fernandes and Burgess, 2006; Fernandes et al., 2009a). Whole rock Sm-Nd dating of LAP 02205 has resulted in an age of 2.992 (± 0.025) Ga (Rankenburg et al., 2007). And a U-Pb age based on several in situ analyses of phosphates yields an age of 2.929 Ga (Fig. 17; Anand et al., 2005, 2006). This is clearly a young mare basalt.

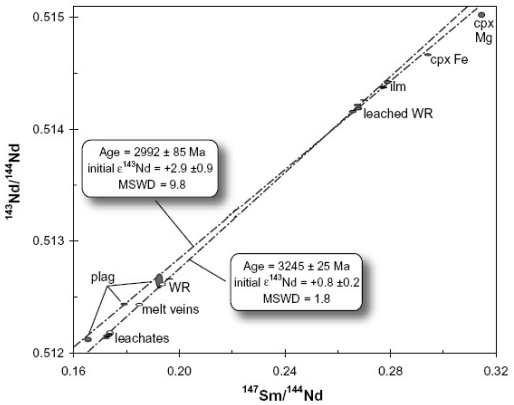

Figure 16: Sm-Nd whole rock and mineral separate isochron for LAP 02205 (from Rankenburg et al., 2007).

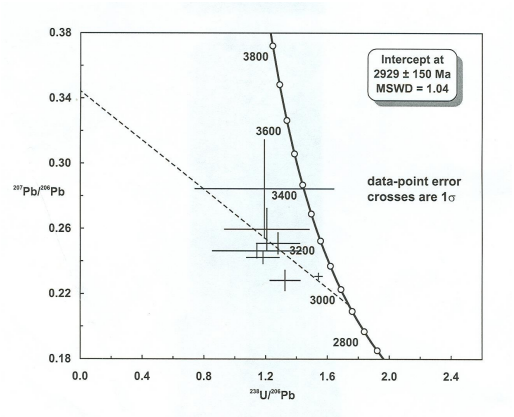

Figure 17: A 3D linear regression of apatite U/Pb measurements for the lunar meteorite LAP 02205 (Anand et al., 2005, 2006).

Cosmogenic isotopes and exposure ages

Measurements of ^{10}Be, ^{26}Al, ^{36}Cl, and ^{41}Ca indicate that the LaPaz basalts were ejected from the Moon 55 (±5) Ka

ago, and fell to Antarctica 20 (±5) Ka ago (Nishiizumi et al., 2006). Together with compositional and textural links, these ages are consistent with launch pairing of the NWA 032 (and paired samples) and LAP 02205 (and paired samples) lunar basalts.

Table 3: **Chemical composition of stones paired with LAP 02205**

reference	2	2	2	2	2	2	2	2	2	2	2	2	2
sample	02224	02224	02224	02226	02226	02226	02436	02436	02436	03632	03632	03632	03632
weight	27.9	27.3	28.8	28.3	27.7	30.5	27.3	26.9	33.3	32.4	34.1	37.3	38.8
split	9-1	19-1	20-1	6-1	10-1	12-1	7-1	9-1	12-1	7-1	7-2	13-1	13-2
technique	d,e	d,e	d,e	d,e	d,e	d,e	d,e	d,e	d,e	d,e	d,e	d,e	d,e
SiO_2 %	45.3	45.0	45.7	45.8	45.6	45.7	45.8	45.4	44.9				
TiO_2	2.98	3.33	2.65	3.23	3.19	3.22	2.81	2.74	2.77				
Al_2O_3	10.40	9.35	9.76	9.50	9.78	9.16	10.67	9.37	9.37				
Cr_2O_3	0.29	0.30	0.36	0.31	0.30	0.31	0.33	0.38	0.42	0.23	0.33	0.31	0.28
FeO	22.7	23.1	21.5	21.8	21.7	21.9	20.9	21.8	22.8	21.8	22.6	22.3	22.8
MnO	0.26	0.28	0.28	0.28	0.28	0.29	0.25	0.28	0.27				
MgO	5.76	6.56	7.49	6.72	6.45	7.10	6.30	7.93	7.74				
CaO	11.2	10.9	11.1	11.1	11.4	11.1	11.4	11.0	10.5				
Na_2O	0.36	0.36	0.37	0.37	0.37	0.37	0.37	0.35	0.35	0.39	0.37	0.38	0.37
K_2O	0.10	0.08	0.06	0.06	0.07	0.06	0.08	0.05	0.06				
P_2O_5	0.12	0.13	0.09	0.09	0.12	0.11	0.13	0.09	0.11				
S %													
sum	99.5	99.3	99.4	99.3	99.3	99.3	99.0	99.4	99.3				
Sc ppm	60.2	58.1	58.8	60.0	60.8	58.4	61.7	60.8	56.8	59.2	58.5	60.4	59.1
V													
Cr	1982	2070	2470	2150	2040	2100	2240	2580	2840	1590	2280	2100	1930
Co	38.5	37.1	38.5	35.5	35.0	37.8	34.3	41.5	42.7	31.5	38.7	37.7	37.0
Ni													
Cu													
Zn													
Ga													
Ge													
As													
Se													
Rb													
Sr	140	140	130	140	140	100	130	130	130	100	140	100	130
Y													
Zr	130	190	190	180	150	220	190	100	170	200	140	160	210
Nb													
Mo													
Ru													
Rh													
Pd ppb													
Ag ppb													
Cd ppb													
In ppb													

Sn ppb													
Sb ppb													
Te ppb													
Cs ppm													
Ba	153	163	144	144	157	142	139	86	126	157	163	128	163
La	12.5	14.5	11.4	11.8	12.7	12.4	11.0	10.6	11.8	13.6	12.7	11.7	13.2
Ce	33.6	38.8	30.8	32.9	34.5	34.4	31.9	27.3	31.6	36.9	33.8	32.1	36.2
Pr													
Nd	22	25	16	18	26	24	18	20	19	22	21	26	23
Sm	7.48	8.61	6.84	7.24	7.62	7.42	6.80	6.32	7.05	8.13	7.58	7.15	7.91
Eu	1.21	1.30	1.12	1.19	1.25	1.22	1.20	1.02	1.14	1.28	1.20	1.20	1.27
Gd													
Tb	1.73	2.03	1.66	1.68	1.77	1.73	1.67	1.51	1.65	1.85	1.76	1.65	1.83
Dy													
Ho													
Er													
Tm													
Yb	6.5	7.3	6.0	6.2	6.6	6.4	5.9	5.3	6.1	7.0	6.5	6.3	6.8
Lu	0.91	1.00	0.82	0.87	0.91	0.90	0.84	0.73	0.86	1.00	0.91	0.89	0.95
Hf	5.67	6.33	5.04	5.25	5.65	5.49	5.01	4.18	5.19	5.97	5.59	5.18	5.85
Ta	0.74	0.80	0.61	0.70	0.73	0.75	0.63	0.57	0.63	0.76	0.76	0.67	0.69
W ppb													
Re ppb													
Os ppb													
Ir ppb													
Pt ppb													
Au ppb													
Th ppm	2.13	2.39	1.80	1.87	2.11	2.04	1.91	1.42	2.00	2.34	1.96	1.96	2.17
U ppm	0.48	0.64	0.44	0.51	0.54	0.43	0.44	0.37	0.56	0.57	0.42	0.55	0.59

technique (a) ICP-AES, (b) ICP-MS, (c) IDMS, (d) Ar, (e) INAA, (f) RNAA, (g) SSMS, (h) fused bead EMPA

Table 3: **Chemical composition of stones paired with LAP 02205 (continued)**

reference	5	5	5	5	5	2	5
sample	02224	02224	02226	02436	03632	LAP	LAP
weight	27.9	27.3	28.8	28.3	27.7	641	?
split	17	18	13	20	8	avg	avg
technique	d,e	d,e	d,e	d,e	d,e	d,e	d,e
SiO_2 %	45.9	45.3	45.3	45.3	45.7	45.3	45.6
TiO_2	2.94	3.27	3.20	3.23	3.26	3.11	3.17
Al_2O_3	9.45	9.95	10.07	9.52	9.65	9.79	9.76
Cr_2O_3	0.32	0.30	0.31	0.36	0.33	0.31	0.32
FeO	22.1	22.0	22.0	22.1	21.7	22.2	21.9
MnO	0.31	0.29	0.30	0.30	0.31	0.29	0.31
MgO	7.19	6.84	6.84	7.71	7.25	6.63	7.02
CaO	11.1	11.3	11.2	10.8	11.2	11.09	11.2
Na_2O	0.35	0.38	0.35	0.33	0.33	0.38	0.36
K_2O	0.10	0.11	0.10	0.08	0.08	0.07	0.10
P_2O_5	0.17	0.16	0.16	0.13	0.12	0.10	0.15
SO_3	0.16	0.14	0.15	0.15	0.17		0.15
sum	100	100	100	100	100	99.28	100
Sc ppm	59.2	57.3	58.8	54.0	58.4	59.2	
V	114	109	110	110	113		
Cr	2368	2172	2192	2298	2300	2096	
Co	37.6	36.9	36.9	37.5	37.9	37.0	
Ni	20.6	18.5	21.9	26.0	21.8		
Cu	19.8	19.4	18.6	16.4	19.8		
Zn	30.8	29.6	27.1	26.3	30.2		
Ga	4.29	4.07	4.18	3.58	4.28		
Ge							
As							
Se							
Rb	1.86	1.74	1.82	1.50	1.79		
Sr	124	122	122	104	124	133	
Y	64.9	64.9	64.0	55.1	64.5		
Zr	194	190	185	161	189	183	
Nb	13.3	12.9	12.8	11.1	13.2		
Mo							
Ru							
Rh							
Pd ppb							
Ag ppb							
Cd ppb							
In ppb							
Sn ppb							
Sb ppb							
Te ppb							
Cs ppm	0.04	0.04	0.04	002	0.02		

Ba	137	131	134	112	134	145
La	11.4	11.5	11.5	10.2	11.5	13.1
Ce	29.6	29.3	30.6	25.3	29.8	34.7
Pr	4.57	4.5	4.67	3.93	4.61	
Nd	21.5	21.5	21.9	18.6	21.6	22
Sm	6.75	6.73	6.79	5.84	6.87	7.74
Eu	1.10	1.07	1.11	0.93	1.13	1.24
Gd	9.08	8.73	8.92	7.57	9.04	
Tb	1.64	1.62	1.65	1.41	1.64	1.79
Dy	10.6	10.4	10.6	9.1	10.6	
Ho	2.30	2.21	2.28	1.94	2.28	
Er	6.09	6.04	6.08	5.26	6.10	
Tm	0.95	0.94	0.95	0.82	0.96	
Yb	5.95	5.91	5.92	5.12	5.97	6.59
Lu	0.93	0.90	0.91	0.79	0.92	0.92
Hf	5.02	4.92	4.90	4.25	5.00	5.58
Ta	0.68	0.65	0.65	0.57	0.67	0.71
W ppb						
Re ppb						
Os ppb						
Ir ppb						
Pt ppb						
Au ppb						
Th ppm	2.04	2.04	2.06	1.72	2.03	2.04
U ppm	0.49	0.50	0.50	0.43	0.49	0.52

Processing

LAP 02205 was initially processed in the summer of 2003, generating splits ,1 ,2 ,3 and ,4 (Figs. 18, 19, 20). Later allocations in the Fall of 2003 resulted in extensive subdivision of ,2 (Fig. 21 and Table 4).

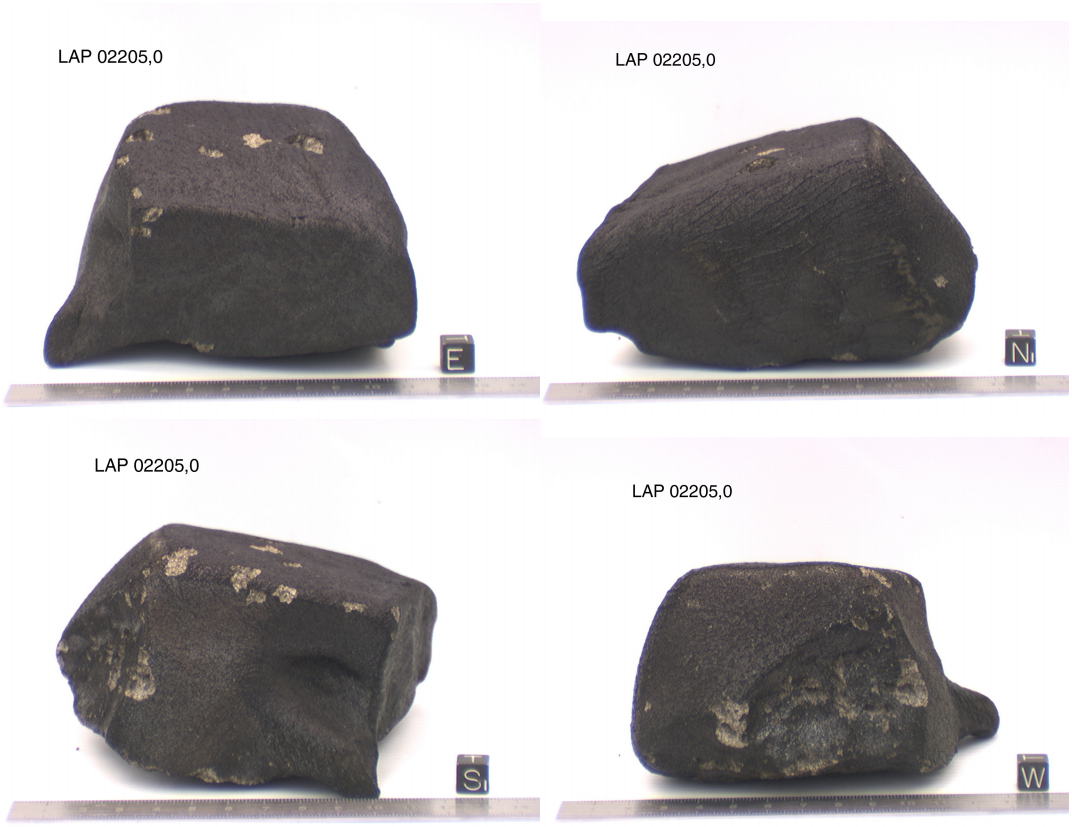

Figure 18: Four laboratory views of LAP 02205 with 1 cm orientation cube for scale.

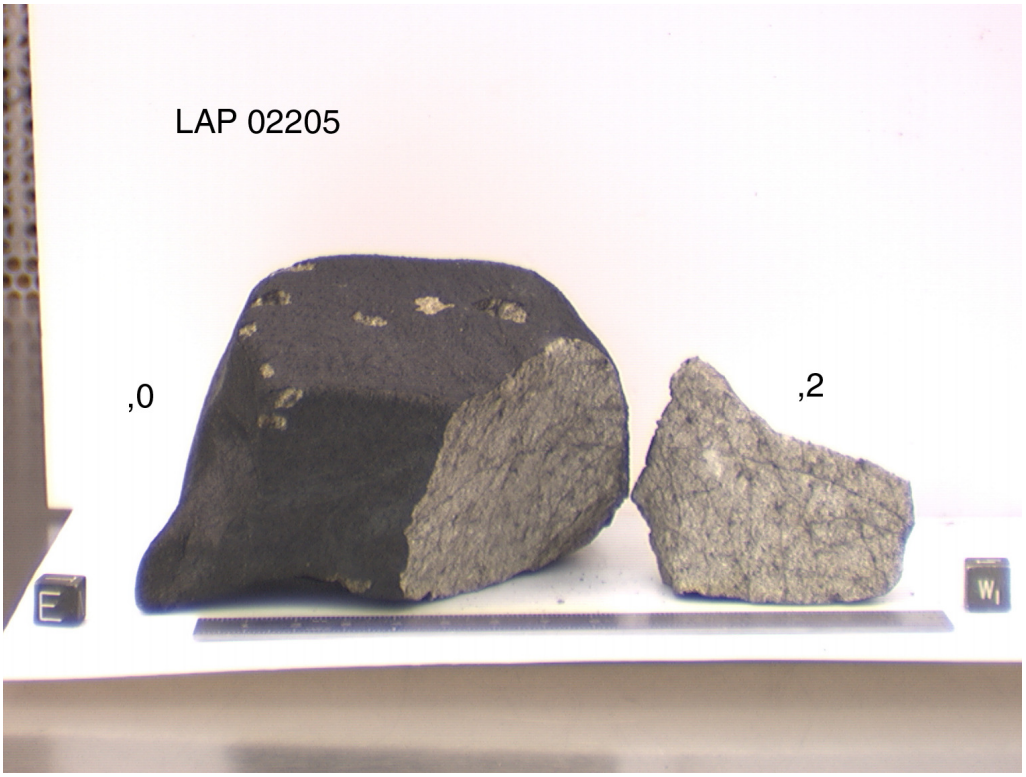

Figure 19: Initial processing of LAP 02205, showing splits ,0 and ,2. Cubes are 1 cm.

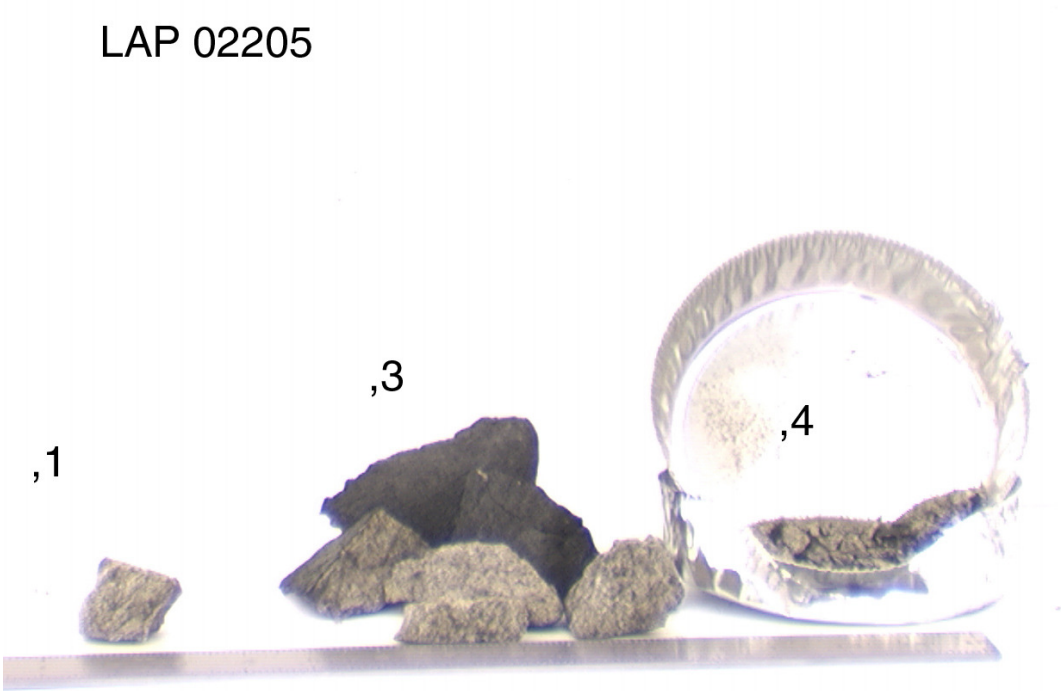

Figure 20: LAP 02205, 1 ,3 and ,4. Most allocations have been derived from these splits 1, 2 and 3 (see Table 3).

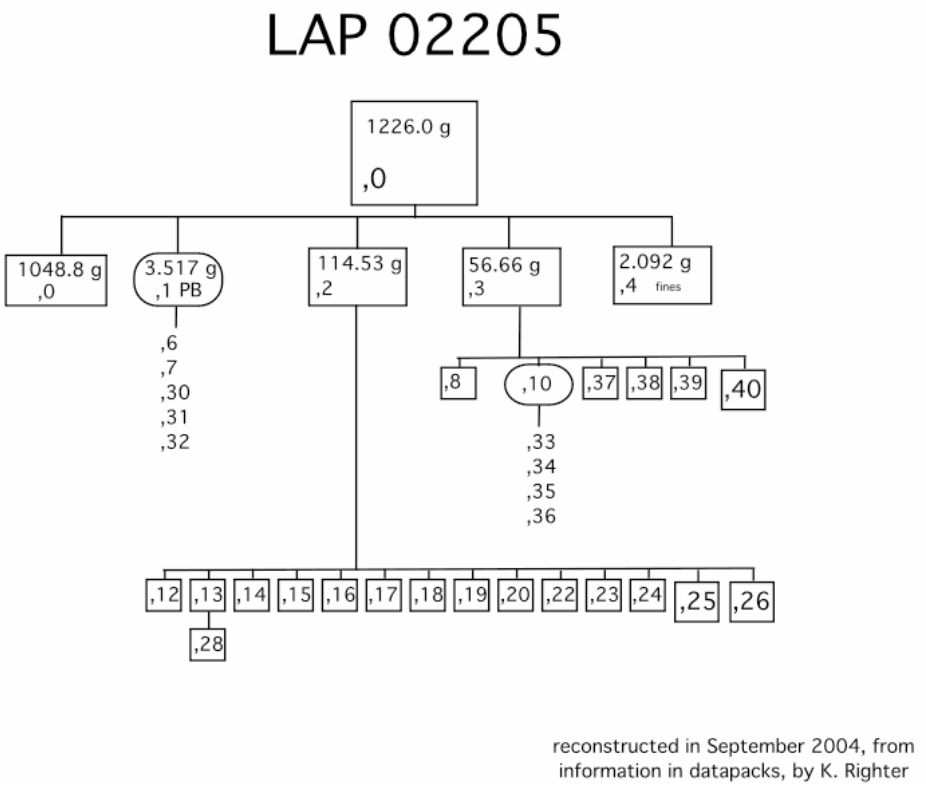

Figure 21: Genealogy of LAP 02205 based on information available in datapacks at JSC.

Table 4: Split allocations of LAP 02205 (1/10)

Split	parent	Mass (g)	PI or location	comment
0	-	1048	JSC	(as of January 2010)
1	0	3.467	Potted butt	Potted butt
2	0	97.044	JSC	Documented pc
3	0	49.358	JSC	chips
6	1	0.01	McCoy/SI	Thin section
7	1	0.01	JSC	Thin section
8	3	0.107	R.N. Clayton	Int chip
12	2	0.016	Bizarro	Int chip
13	2	0.209	JSC	Int chip
14	2	0.345	Nyquist	Int chip
15	2	0.652	Nishiizumi	Ext.
16	2	0.484	Mikouchi	Int chip
17	2	0.535	Nishiizumi	Int chip
18	2	0.318	Brandon	Int chip
19	2	1.572	L.A. Taylor	Int chip
20	2	0.258	Korotev	Int chip
22	2	0.403	Nishiizumi	Ext. chip
23	2	4.66	Brandon	Int chip

24	2	0.265	Korotev	Int chip
28	13	0.099	Arai	Int chip
30	1	0.01	Brandon	Thin section
31	1	0.01	L.A. Taylor	Thin section
32	1	0.01	S. Russell	Thin section
33	10	0.01	Korotev	Thin section
34	10	0.01	Mikouchi	Thin section
35	10	0.01	Arai	Thin section
36	10	0.01	L.A.Taylor	Thin section
37	3	0.334	Busemann	Int chip
38	3	0.15	Herzog	Int chip
39	3	0.172	Herzog	Int chip
42	1	0.01	Righter	Thick section
44	21	0.056	S. Russell	Int chip
49	40	0.566	Moynier	Int chip
51	47	0.01	JSC	Thin section
52	48	0.01	JSC	Thin section
53	48	0.07	Lee	Thick section
54	2	21.248	McCoy	Int chip
58	55	1.008	Fernandes	Int chip
61	59	0.1	Fernandes	Thin section
62	59	0.01	Hallis	Thick section
63	55	0.319	Pieters	2 chips
64	55	0.23	Nishiizumi	Int chip
66	55	0.428	Herzog	Int chip
68	55	0.223	Moynier	Int chip